International Journal of Signal Processing, Image Processing and Pattern Recognition
Vol.8, No.11 (2015), pp.85-98
http://dx.doi.org/10.14257/ijsip.2015.8.11.09

Switching-Based SVPWM Control for Three-Phase Active Power Filter

Zhang Menghua[*1], Cheng Xingong[2], Zong Xiju[3], and Zhang Yong[4]

School of Electronic and Engineering, University of Jinan, Shandong, Jinan, 250022, China
menghuahappy@163.com

Abstract

A switching-based SVPWM control method for three-phase active power filter is proposed in this paper. First, error model of the switched system is established. And then, according to the space voltage vector diagram and three-phase supply voltage waveforms, the supply voltage is divided into six sectors. In each sector, a combination of switching subsystem is set up according to the requirement of quadratic stability condition. Finally, the common Lyapunov function is selected and therefore, the subsystem is determined, which has minimum derivative of Lyapunov function and meets the conditions above. The validity of the proposed control method is proved with Matlab/Simulink and experimental results.

Keywords: *Active power filter, quadratic stability, space voltage vector control, convex combination, Lyapunov function, switched system*

1. Introduction

With the rapid development of power electronics technology, more and more power electronic equipment's for industry and people's daily lives are coming out. At the same time, power electronics produce serious harmonic pollution problems to the power grid. As is well-known, the power system harmonic content is an important indicator of power quality. In order to reduce the harmonic level of power system, a growing number of scholars have made a study focusing on this [1]. The active power filter (APF) plays an important role in harmonic compensation increasingly, and the associated control algorithm is one of the core issues emerged in the harmonic compensation.

Linearization and unified modeling is the basic idea of investigating APF. In other words, averaging of each switching mode in the time domain, the corresponding period average mode is obtained [2-3].Dead-beat control [4], one-cycle control [5], the method of current tracking control proposed in [6-7], and sliding mode variable structure methods [8] were all based on period average model. However, APF is a typical nonlinear hybrid dynamic system, so we can get nothing but the macro level performance of APF. Meanwhile, nonlinear systems of APF can be divided into multiple linear dynamic subsystems by on-off control. By the advantage of the switching control theory, Zongbo Hu and Willem applied switched linear systems theory to the controllability and reachability of dc-dc converters, and they made great progress [9-11]. The control strategy of single phase APF as switched linear systems was proposed in [12]. In literature [13] the switching model for APF was established and the equivalent discrete system model was obtained, but the corresponding calculation process was very complicated.

So a method combined switching control method with space voltage vector control algorithm was proposed in this paper. Three-phase power supply voltage is divided into 6 sectors. And then according to the Lyapunov function and the requirement of quadratic stability condition, a switching rule is proposed to simplify the algorithm. Due to the reasonable use of zero-vector, switching loss decreases significantly.

ISSN: 2005-4254 IJSIP

2. Error Model of Active Power Filter Switched System

The error model of three-phase APF is illustrated in Figure 1.

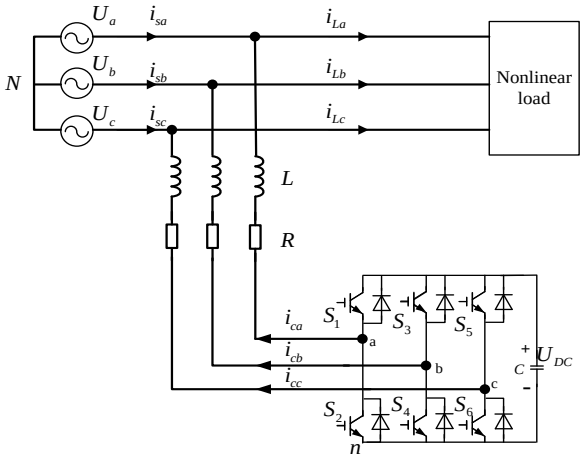

Figure 1. Topological Structure of Three-Phase APF

APF is in parallel with the nonlinear load and supplies compensation currents to cancel the harmonic current components from the source current i_{sj} *(j=a,b,c)*. i^*_{cj} *(j=a,b,c)* is the harmonic current generated by the nonlinear load, namely the reference current. Through switching the IGBTs, APF can generate compensation current i_{cj}*(j=a,b,c)* that tracks i^*_{cj} *(j=a,b,c)* to make the source current nearly sinusoidal. L stands for the filter inductor, R for the total equivalent resistance of the filter inductors. The voltage source of APF is U_{DC}.

Define switching coefficient:

$$S_k = \begin{cases} 1 & \text{the positive switch is on and the negative switch is off} \\ 0 & \text{the negative switch is on and the positive switch is off} \end{cases}$$

The 8 switching modes of active power filter are shown in Table 1:

Table 1. Switching Modes of Three-Phase APF

Switching modes	S_a	S_b	S_c
Ⅰ	0	0	0
Ⅱ	0	0	1
Ⅲ	0	1	0
Ⅳ	0	1	1
Ⅴ	1	0	0
Ⅵ	1	0	1
Ⅶ	1	1	0
Ⅷ	1	1	1

From Figure 1, according to Kirchhoff Voltage Law, it can be obtained that:

$$\begin{cases} u_{aN} = R i_{ca} + L \dfrac{d i_{ca}}{d t} + U_a \\ u_{bN} = R i_{cb} + L \dfrac{d i_{cb}}{d t} + U_b \\ u_{cN} = R i_{cc} + L \dfrac{d i_{cc}}{d t} + U_c \end{cases} \tag{1}$$

where u_{aN}, u_{bN} and u_{cN} represent voltage drop between points a,b,c and neutral point N, respectively.

In the case of symmetrical load, it holds:

$$u_{aN} + u_{bN} + u_{cN} = 0 \tag{2}$$

and

$$\begin{cases} u_{aN} = u_{an} + u_{nN} \\ u_{bN} = u_{bn} + u_{nN} \\ u_{cN} = u_{cn} + u_{nN} \end{cases} \tag{3}$$

Substituting (2-3) into (1), it follows that:

$$u_{nN} = -\frac{1}{3}\left(S_a U_{DC} + S_b U_{DC} + S_c U_{DC} \right) \tag{4}$$

Substituting (3-4) into (2), it follows that:

$$\begin{cases} u_{aN} = \dfrac{2S_a - S_b - S_c}{3} U_{DC} \\ u_{bN} = \dfrac{2S_b - S_a - S_c}{3} U_{DC} \\ u_{cN} = \dfrac{2S_c - S_a - S_b}{3} U_{DC} \end{cases} \tag{5}$$

Since the change rate of U_{DC} is much less than that of APF output current, we consider U_{DC} as a constant. Then the state equation of the system is obtained:

$$\begin{bmatrix} \dfrac{d i_{ca}}{d t} \\ \dfrac{d i_{cb}}{d t} \\ \dfrac{d i_{cc}}{d t} \end{bmatrix} = \begin{bmatrix} -\dfrac{\mathrm{R}}{\mathrm{L}} & 0 & 0 \\ 0 & -\dfrac{\mathrm{R}}{\mathrm{L}} & 0 \\ 0 & 0 & -\dfrac{\mathrm{R}}{\mathrm{L}} \end{bmatrix} \begin{bmatrix} i_{ca} \\ i_{cb} \\ i_{cc} \end{bmatrix} + \begin{bmatrix} -\dfrac{2S_a - S_b - S_c}{3\mathrm{L}} U_{DC} + \dfrac{U_a}{\mathrm{L}} \\ -\dfrac{2S_b - S_a - S_c}{3\mathrm{L}} U_{DC} + \dfrac{U_b}{\mathrm{L}} \\ -\dfrac{2S_c - S_a - S_b}{3\mathrm{L}} U_{DC} + \dfrac{U_c}{\mathrm{L}} \end{bmatrix} = \boldsymbol{A}\boldsymbol{x} + \boldsymbol{B}_i \qquad i = 1, 2, \cdots, 8 \tag{6}$$

where $x=[i_{ca}\ \ i_{cb}\ \ i_{cc}]^T$ stands for the state variable. Suppose that $x_d=[x_{d1}\ \ x_{d2}\ \ x_{d3}]^T$ is the reference value of compensation current, which is also the switching equilibrium point. Introduce a coordinate transformation $\Delta x_d = x - x_d$. So $\Delta x_d = 0$ is the new switching equilibrium point. Then the error model of the switched system is obtained:

$$\begin{aligned}\Delta\dot{\boldsymbol{x}} &= \begin{bmatrix} -\frac{R}{L} & 0 & 0 \\ 0 & -\frac{R}{L} & 0 \\ 0 & 0 & -\frac{R}{L} \end{bmatrix} \Delta\boldsymbol{x} + \begin{bmatrix} -\frac{2S_a - S_b - S_c}{3L}U_{DC} + \frac{U_a}{L} - \frac{R}{L}x_{d1} \\ -\frac{2S_b - S_a - S_c}{3L}U_{DC} + \frac{U_b}{L} - \frac{R}{L}x_{d2} \\ -\frac{2S_c - S_a - S_b}{3L}U_{DC} + \frac{U_c}{L} - \frac{R}{L}x_{d3} \end{bmatrix} \\ &= \boldsymbol{A}\Delta\boldsymbol{x} + \boldsymbol{b}_i \qquad i = 1,2,\cdots,8 \end{aligned} \tag{7}$$

where $\Delta x=[\Delta i_{ca}\ \Delta i_{cb}\ \Delta i_{cc}]^T$ stands for state variable. We can see that system matrix A is fixed and $A<0$ for three- phase active power filter.

3. Quadratic Stability based Switching Control of the Three-Phase Active Power Filter

The main result of this paper is as follows:

Theorem 1: If there exists a convex combination $\lambda=[\lambda_1 \ldots \lambda_m]^T$ for $m\in[2,8]$, such that:

$$\begin{cases} \sum_{j=1}^{m} \lambda_j = 1 \\ \lambda_j \in (0,1) \\ D_i\boldsymbol{A} + D_i^{-}\boldsymbol{G} < 0 \\ \left(D_i\boldsymbol{A} + D_i^{-}\boldsymbol{G}\right)x_d + D_i^{-}\boldsymbol{G}\boldsymbol{B}_\lambda = 0 \end{cases} \tag{8}$$

The state-switching control,

$$\sigma(t) = \arg \min_i \Delta\boldsymbol{x}^T\boldsymbol{b}_i \tag{9}$$

makes the equilibrium solution $\Delta x_d = 0$ of (6) globally asymptotically stable.

Proof: Choose Lyapunov function

$$\boldsymbol{V}(\boldsymbol{x}) = \frac{1}{2}\Delta\boldsymbol{x}^T\Delta\boldsymbol{x} \tag{10}$$

The derivative of (10) can be obtained that,

$$\begin{aligned}\dot{\boldsymbol{V}}(\boldsymbol{x}) &= \frac{1}{2}\left(\Delta\dot{\boldsymbol{x}}^T\right)\Delta\boldsymbol{x} + \frac{1}{2}\Delta\boldsymbol{x}^T\Delta\dot{\boldsymbol{x}} \\ &= \Delta\boldsymbol{x}^T\left(\boldsymbol{A}\Delta\boldsymbol{x} + \boldsymbol{b}_i\right) = \Delta\boldsymbol{x}^T\boldsymbol{A}\Delta\boldsymbol{x} + \Delta\boldsymbol{x}^T\boldsymbol{b}_i \end{aligned} \tag{11}$$

where $A<0$, thus $\Delta x^TA\Delta x<0$, $m\in[2\text{-}8]$. Because there exists a convex combination $\lambda=[\lambda_1 \ldots \lambda_m]^T$ subject to $b_\lambda=0$, according to [14], $\min_i \Delta\boldsymbol{x}^T\boldsymbol{b}_i \le 0$, then $\dot{\boldsymbol{v}}(\boldsymbol{x}) < 0$. The theorem is proved.

Corollary 1: If there exists a convex combination $\lambda=[\lambda_1 \ldots \lambda_m]^T$ for $m\in[2,8]$ such that

$$\begin{cases} \sum_{j=1}^{m} \lambda_j = 1 \\ \lambda_j \in (0,1) \\ D_i \boldsymbol{A} + D_i^{-} \boldsymbol{G} < 0 \\ \left(D_i \boldsymbol{A} + D_i^{-} \boldsymbol{G}\right) x_d + D_i^{-} \boldsymbol{G} \boldsymbol{B}_\lambda = 0 \end{cases} \tag{12}$$

The state-switching control,

$$\sigma(t) = \arg \min_i \Delta \boldsymbol{x}^T \boldsymbol{c}_i \tag{13}$$

makes the equilibrium solution $\Delta x_d = 0$ of (6) globally asymptotically stable, where:

$$\boldsymbol{c}_i = \begin{bmatrix} -\frac{2S_a - S_b - S_c}{3\mathrm{L}} U_{DC} \\ -\frac{2S_b - S_a - S_c}{3\mathrm{L}} U_{DC} \\ -\frac{2S_c - S_a - S_b}{3\mathrm{L}} U_{DC} \end{bmatrix} \tag{14}$$

Proof: Noting that:

$$\begin{aligned} &\Delta \boldsymbol{x}^T \boldsymbol{b} \\ &= \begin{bmatrix} \frac{d\Delta i_{ca}}{dt} \\ \frac{d\Delta i_{cb}}{dt} \\ \frac{d\Delta i_{cc}}{dt} \end{bmatrix}^T \begin{bmatrix} -\frac{2S_a - S_b - S_c}{3\mathrm{L}} U_{DC} + \frac{U_a}{\mathrm{L}} - \frac{\mathrm{R}}{\mathrm{L}} x_{d1} \\ -\frac{2S_b - S_a - S_c}{3\mathrm{L}} U_{DC} + \frac{U_b}{\mathrm{L}} - \frac{\mathrm{R}}{\mathrm{L}} x_{d2} \\ -\frac{2S_c - S_a - S_b}{3\mathrm{L}} U_{DC} + \frac{U_c}{\mathrm{L}} - \frac{\mathrm{R}}{\mathrm{L}} x_{d3} \end{bmatrix} \\ &= \begin{pmatrix} -\frac{d\Delta i_{ca}}{dt}\frac{2S_a - S_b - S_c}{3\mathrm{L}} - \frac{d\Delta i_{cb}}{dt}\frac{2S_b - S_a - S_c}{3\mathrm{L}} \\ -\frac{d\Delta i_{cc}}{dt}\frac{2S_c - S_a - S_b}{3\mathrm{L}} \end{pmatrix} U_{DC} + \begin{pmatrix} \frac{d\Delta i_{ca}}{dt}\frac{U_a}{\mathrm{L}} + \frac{d\Delta i_{cb}}{dt}\frac{U_b}{\mathrm{L}} + \frac{d\Delta i_{cc}}{dt}\frac{U_c}{\mathrm{L}} - \\ \frac{d\Delta i_{ca}}{dt}\frac{\mathrm{R}}{\mathrm{L}} x_{d1} - \frac{d\Delta i_{cb}}{dt}\frac{\mathrm{R}}{\mathrm{L}} x_{d2} - \frac{d\Delta i_{cc}}{dt}\frac{\mathrm{R}}{\mathrm{L}} x_{d3} \end{pmatrix} \\ &= \Delta x^T c_i + d \end{aligned} \tag{15}$$

For each subsystem, d is always the same. Thus it can be obtained that:

$$\sigma(t) = \arg \min_i \Delta \boldsymbol{x}^T \boldsymbol{b}_i = \arg \min_i \Delta \boldsymbol{x}^T \boldsymbol{c}_i \tag{16}$$

Corollary 1 is equivalent to theorem 1 with simplified calculation process.

4. Switching-based SVPWM Control

From (6) it can be obtained,

$$\begin{bmatrix} U_a \\ U_b \\ U_c \end{bmatrix} = \mathrm{L} \begin{bmatrix} \frac{di_{ca}}{dt} \\ \frac{di_{cb}}{dt} \\ \frac{di_{cc}}{dt} \end{bmatrix} + \mathrm{R} \begin{bmatrix} i_{ca} \\ i_{cb} \\ i_{cc} \end{bmatrix} + \begin{bmatrix} \frac{2S_a - S_b - S_c}{3\mathrm{L}} U_{DC} \\ \frac{2S_b - S_a - S_c}{3\mathrm{L}} U_{DC} \\ \frac{2S_c - S_a - S_b}{3\mathrm{L}} U_{DC} \end{bmatrix} \tag{17}$$

Because the voltages of L and R are far less than the power supply voltage, they can be ignored. (17) can be simplified as:

$$\begin{bmatrix} U_a \\ U_b \\ U_c \end{bmatrix} = \frac{U_{DC}}{3} \begin{bmatrix} 2 & -1 & -1 \\ -1 & 2 & -1 \\ -1 & -1 & 2 \end{bmatrix} \begin{bmatrix} S_a \\ S_b \\ S_c \end{bmatrix} \tag{18}$$

As the right hand side of (18) is the reference input of SVPWM, U_a , U_b and U_c can be regarded as the SVPWM reference input. Figure 2 shows the waveform of three-phase power supply voltage, which is divided equally into 6 sectors.

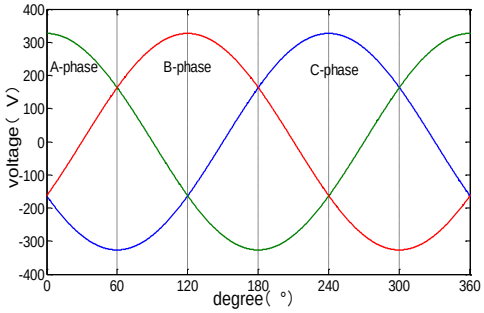

Figure 2. Waveform of Three-Phase Power Supply Voltage

In the interval [0°, 120°], U_c is the minimum of the three-phase voltages. Let S_c=0. In the same way, S_b =0 and S_b =0 is set correspondingly in interval [120°, 240°] and [240°, 360°].

The voltage space vector graph constituted of U_a, U_b, and U_c is shown in Figure 3.

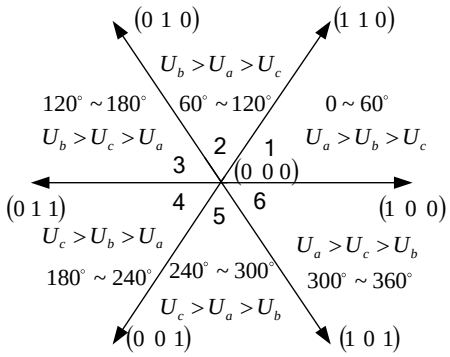

Figure 3. Voltage Space Vector Graph

Within interval [0°, 60°], namely sector 1, only two bridge legs S_1~ S_2 and S_3~ S_4 act for S_c=0. The system can be treated as four switching linear subsystems I, II, III and IV in accordance with the evolution of S_a, S_b, S_c and the switching modes of each subsystem is listed in Table 1. For purpose of reducing the switching loss, two groups of switch sequence are chosen, I, III, VII and I, V, VII. Take the sequence I, V, VII for example.

When S_a=0, S_b=0, S_c=0

$$\boldsymbol{b}_1 = \begin{bmatrix} \frac{U_a}{\mathrm{L}} - \frac{\mathrm{R}}{\mathrm{L}} x_{d1} \\ \frac{U_b}{\mathrm{L}} - \frac{\mathrm{R}}{\mathrm{L}} x_{d2} \\ \frac{U_c}{\mathrm{L}} - \frac{\mathrm{R}}{\mathrm{L}} x_{d3} \end{bmatrix} \tag{19}$$

When S_a=1, S_b=0, S_c=0

$$\boldsymbol{b}_2 = \begin{bmatrix} -\frac{2}{3\mathrm{L}} U_{DC} + \frac{U_a}{\mathrm{L}} - \frac{\mathrm{R}}{\mathrm{L}} x_{d1} \\ \frac{1}{3\mathrm{L}} U_{DC} + \frac{U_b}{\mathrm{L}} - \frac{\mathrm{R}}{\mathrm{L}} x_{d2} \\ \frac{1}{3\mathrm{L}} U_{DC} + \frac{U_c}{\mathrm{L}} - \frac{\mathrm{R}}{\mathrm{L}} x_{d3} \end{bmatrix} \tag{20}$$

When S_a=1, S_b=1, S_c =0,

$$\boldsymbol{b}_3 = \begin{bmatrix} -\frac{1}{3\mathrm{L}} U_{DC} + \frac{U_a}{\mathrm{L}} - \frac{\mathrm{R}}{\mathrm{L}} x_{d1} \\ -\frac{1}{3\mathrm{L}} U_{DC} + \frac{U_b}{\mathrm{L}} - \frac{\mathrm{R}}{\mathrm{L}} x_{d2} \\ \frac{2}{3\mathrm{L}} U_{DC} + \frac{U_c}{\mathrm{L}} - \frac{\mathrm{R}}{\mathrm{L}} x_{d3} \end{bmatrix} \tag{21}$$

We find that $\lambda_1+\lambda_2+\lambda_3=1(\lambda_i \in (0,1),\ i=1,2,3)$ is always true which can derive $b_\lambda=0$, whose expanded form is:

$$\begin{cases} \lambda_1 \left(\frac{U_a}{\mathrm{L}} - \frac{r}{\mathrm{L}} x_{d1} \right) + \lambda_2 \left(-\frac{2}{3\mathrm{L}} U_{DC} + \frac{U_a}{\mathrm{L}} - \frac{\mathrm{R}}{\mathrm{L}} x_{d1} \right) \\ \qquad + \lambda_3 \left(-\frac{1}{3\mathrm{L}} U_{DC} + \frac{U_a}{\mathrm{L}} - \frac{\mathrm{R}}{\mathrm{L}} x_{d1} \right) = 0 \\ \lambda_1 \left(\frac{U_b}{\mathrm{L}} - \frac{r}{\mathrm{L}} x_{d2} \right) + \lambda_2 \left(\frac{1}{3\mathrm{L}} U_{DC} + \frac{U_b}{\mathrm{L}} - \frac{\mathrm{R}}{\mathrm{L}} x_{d2} \right) \\ \qquad + \lambda_3 \left(-\frac{1}{3\mathrm{L}} U_{DC} + \frac{U_b}{\mathrm{L}} - \frac{\mathrm{R}}{\mathrm{L}} x_{d2} \right) = 0 \end{cases} \tag{22}$$

We can obtain,

$$\begin{cases} \lambda_1 = 1 - \frac{2(U_a - \mathrm{R} x_{d1}) + (U_b - \mathrm{R} x_{d2})}{U_{DC}} \\ \lambda_2 = \frac{(U_a - \mathrm{R} x_{d1}) - (U_b - \mathrm{R} x_{d2})}{U_{DC}} \\ \lambda_3 = \frac{(U_a - \mathrm{R} x_{d1}) + (2U_b - 2\mathrm{R} x_{d2})}{U_{DC}} \end{cases} \tag{23}$$

satisfying the formula (8) and (12), the condition of theorem 1 and corollary 1, respectively.

In the same way, three switching subsystems meeting the condition of theorem 1 and corollary 1 can be obtained for all other sectors, shown in Table 2.

Table 2. Switching Modes and Switching Functions of Three-Phase APF in Each Sector

Interval	Switching modes	S_a	S_b	S_c
0~60° $U_a>U_b>U_c$ Sector 1	I V Ⅶ	0 1 1	0 0 1	0 0 0
60°~120° $U_b>U_a>U_c$ Sector 2	I Ⅲ Ⅶ	0 0 1	0 1 1	0 0 0
120°~180° $U_b>U_c>U_a$ Sector 3	I Ⅲ Ⅳ	0 0 0	0 1 1	0 0 1
180°~240° $U_c>U_b>U_a$ Sector 4	I Ⅱ Ⅳ	0 0 0	0 0 1	0 1 1
240°~300° $U_c>U_a>U_b$ Sector 5	I Ⅱ Ⅵ	0 0 1	0 0 0	0 1 1
300°~360° $U_a>U_c>U_b$ Sector 6	I V Ⅵ	0 1 1	0 0 0	0 0 1

5. System Simulation and Experimental Verification

In order to verify the performance of the proposed control method, Matlab/Simulink is used to simulate the system. The parameters of this simulation system are given as follows, R=0.05Ω, L=2mH, C=6800μF, System voltage is 380V/50Hz, the reference dc side voltage U_{DC}^{*}=750V. In order to verify the dynamic response performance, we adopt two three-phase uncontrolled rectifiers as the nonlinear loads. DC loads are R=25Ω, C=600μF and R=10Ω, L=10mH, respectively. When t=0.5s, we put the second uncontrolled rectifier into operation.

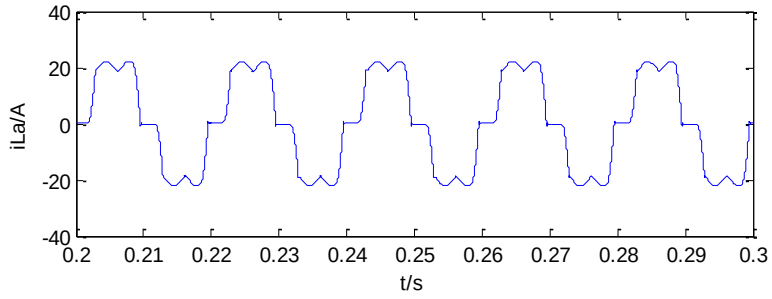

Figure 4. Nonlinear Load Current iLa

The harmonic component of load current is particularly high as shown in Figure 4. It is obvious that there is a serious distortion of current and the THD is 24.31%.

Figure 5 shows the waveform of phase-A supply current after compensation. The near sinusoidal supply current shows that most of the harmonic currents have been compensated successfully. That is to say, the compensation current can track the change of load current harmonic components. We can see from Figure 6 that the THD is only 1.28%.

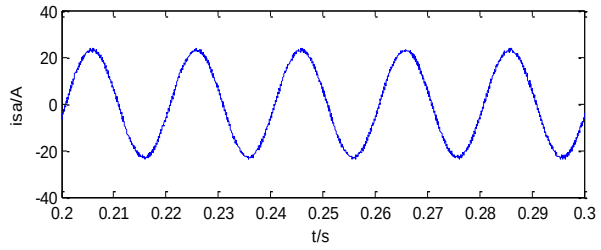

Figure 5. Supply Current i_{sa} after Compensation

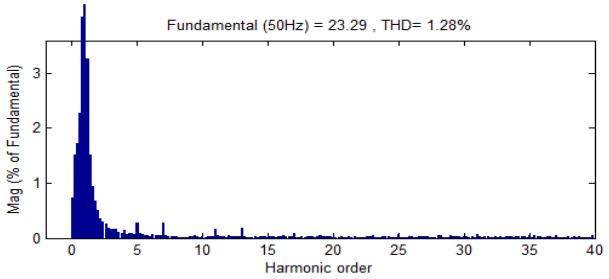

Figure 6. Spectrum Diagram of Supply Current i_{sa} after Compensation

Figure 7 shows the process that compensation current of APF tracks the change of load current harmonic components.

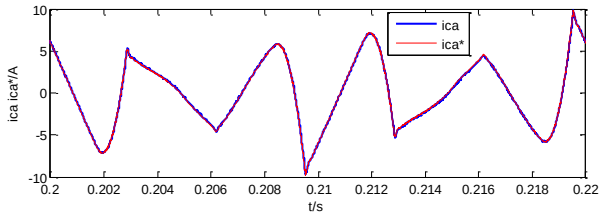

Figure 7. The Compensation Current i_{ca} Tracking Command Current i_{ca}*

Figure 8 shows the waveform of DC-side output voltage.

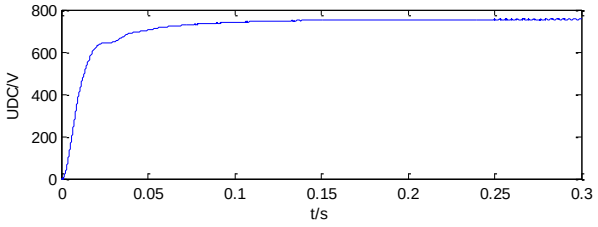

Figure 8. DC-side Output Voltage UDC

Figure 9 shows the Lyapunov function changing over time. We can see from the figure that the system is stable at 0.02s.

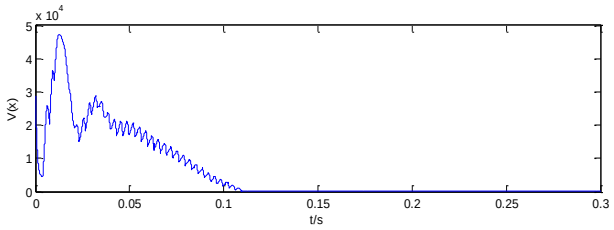

Figure 9. Lyapunov Function V(x)

The waveforms of the load current i_{La} and the system current i_{sa} under saltation load are shown in Figure 10 and Figure 11, respectively. We can see from the figures that in the case of load changing, APF controlled by the method proposed in this paper has a good harmonic compensation effect.

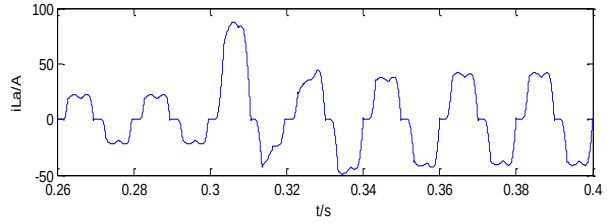

Figure 10. Waveform of the Load Current i_{La} Under Saltation Load

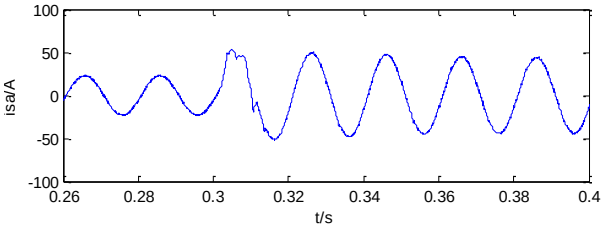

Figure 11. Waveform of the System Current i_{sa} Under Saltation Load

The Driver signals for switches S_a, S_b, S_c are shown in Figure 12. It's shown that when U_c is the minimum, S_c=0. It's to say that only two bridge legs switch, while it requires three bridge legs to switch [14]. So the number of switching needed in the control strategy proposed in the present paper is less. Switching loss then decreases dramatically.

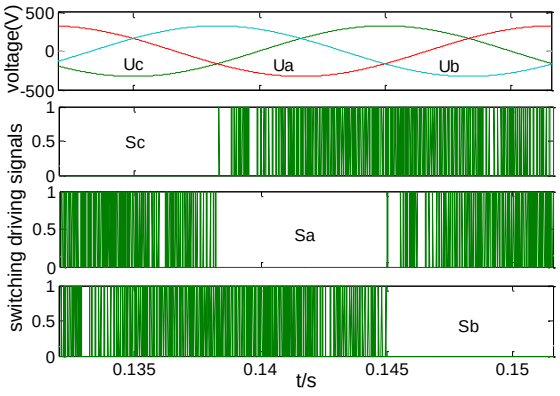

Figure 12. Driver Signals for Switches

For further verifying the validity of the proposed control strategy in this paper, an experimental platform is set up. Type of IGBT is CM300dx of Mitsubishi. Type of DSP is TMS320F28335 of Texas Instruments. Type of FPGA is EP3C10E144C8N of Altera. Switching rules are realized by DSP. The main function of FPGA is protection of hardware circuit, fault detection, control of A/D and so on. We adopt two three-phase uncontrolled rectifiers as the nonlinear load. DC loads are R=25Ω, L=10mH and R=25Ω, L=10mH, respectively. The circuit parameters of the experiment are the same with simulation.

Figure 13 and Figure 14 show the main circuit and controller of APF.

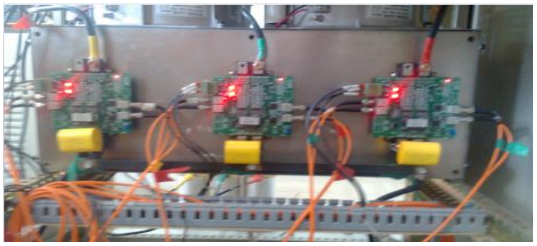

Figure 13. The Main Circuit of APF

Figure 14. The Controller of APF

The waveforms of A-phase load current i_{La}, compensation current i_{ca} and supply current i_{sa} are shown in Figure 15.

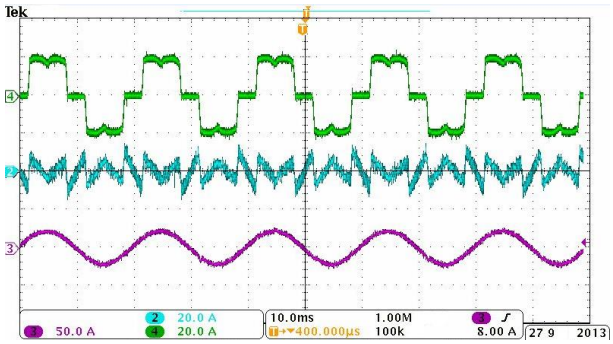

Figure 15. The Waveforms of i_{La}, i_{ca} and i_{sa}

Figure 16 shows the harmonic analysis of three- phase supply current. Due to the limitation of hardware, the sampling period of experimental prototype is larger than the sampling period of simulation. Therefore, the harmonic components of supply current after compensation are not as low as the harmonic components of simulation. We can see from Figure 16, the three-phase THD are 2.9%, 2.9%, 2.8%, respectively.

Figure 16. Harmonic Analysis of Three-Phase Supply Current

Figure 17 shows the dynamic responses to load changing suddenly. After a short time transient process, the APF can compensate harmonic current steady.

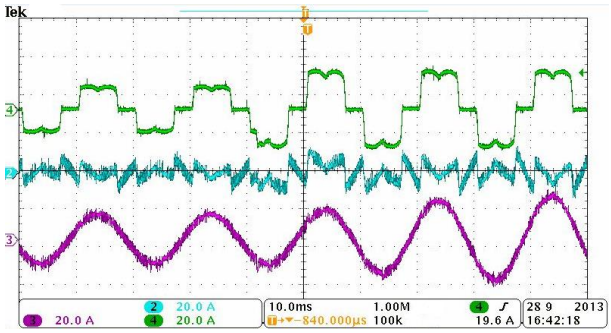

Figure 17. Dynamic Responses to Abrupt Load Change

6. Conclusions

A switching-based SVPWM control method for three-phase active power filter is proposed in this paper. Three-phase power supply voltage is divided into 6 sectors. And then according to the Lyapunov function and the requirement of quadratic stability condition, a switching rule is proposed to simplify the algorithm. Due to the reasonable use of zero-vector, switching loss decreases significantly.

Acknowledgment

This work was supported by the national Natural Scientific Foundation of China (Granted No. 11201179), the Independent Innovation Special Projects of Shandong Province (Granted No. 2012CX30302), and the Natural Science Foundation of Shangdong Province (Granted No.ZR2011EEM024).

References

[1] Z. Y. Li and L. F. Shen "An LCL-APF Direct Power Control Approach Based on Non-Harmonic Detection Technology", Power System Technology, vol. 36, no. 12, **(2012)**, pp. 217-221.
[2] J. Le and Q. R. Jiang, "The analysis of hysteresis current control strategy of three-phase four-wire APF based on the unified mathematic model", Proceeding of the CSEE, vol. 27, no. 10, **(2007)**, pp. 85-91.
[3] J. M. Chen and F. Liu, "Passivity-based controller for three phase four-wire APF", Automation of Electric Power Systems, **(2006)**.
[4] Y. M. Li and W. M. Ma., "Application of deadbeat control in series active power filter", Automation of Electric Power Systems, vol. 25, no. 4, **(2001)**, pp. 28-30.
[5] H. D. Battista and R. J. Mantz., "Harmonic series compensators in power systems: their control via sliding mode", IEEE Transactions on System Control Technology, vol. 8, no.12, **(2000)**, pp. 939-947.
[6] W. P. Zhou, Z. G. Wu and L. Xia, "Current tracking performance optimization control for three-phase three-wire active power filter", Proceedings of the CSEE, vol. 24, no. 11, **(2004)**, pp. 85-90.

[7] S. Fukuda and T. Yoda, "A novel current-tracking method for active filters based on a sinusoidal internal model for PWM inverters", IEEE Trans on Industry Applications, vol. 37, no. 5, **(2001)**, pp. 888-895.
[8] H. H. Tang and C. W. Li, "Modeling and Control of Single Phase Active Power Filter Based on Switched Linear System", Power System Technology, vol. 31, no. 13, **(2007)**, pp. 29-33.
[9] Z. B. Hu, B. Zhang and W. H. Deng, "Controllability and reachability of DC-DC converters as switched linear systems", Proceedings of the CSEE, vol. 24, no. 12, **(2004)**, pp. 165-170.
[10] Z. B. Hu and B. Zhang, "Theoretical analysis and experimental verification of one cycle control feasibility for boost pfc converter", Proceedings of the CSEE, vol. 25, no. 21, **(2005)**, pp.19-23.
[11] L. Willem and K. De, "Digital optimal reduced-order control of pulse-width-modulated switched linear systems", Automatica, vol. 39, no. 11, **(2003)**, pp. 1997-2003.
[12] Y. F. Zhang, X. G. Cheng and X. J. Zong, "Nonlinear switching control of single-phase active power filter", Power System Protection and Control, vol. 39, no.18, **(2011)**, pp. 139-144.
[13] C. W. Li, and H. H. Tang, "Modeling and Quadratic Optimal Control of Three-phase APF Based on Switched System", Proceedings of the CSEE, vol. 28, no. 12, **(2008)**, pp. 66-72.
[14] B. Paolo and S. William, "Quadratic stabilization of a switched affine system about a nonequilibrium point", American Control Conference, **(2004)**, pp. 3890-3895.

Author

Menghua Zhang was born in 1988, she received B.Eng. degree in electrical engineering from University of Jinan, Jinan, China, in 2010. She is currently pursuing the M.S. degree in University of Jinan, Jinan, China. She is major in control engineering.